Phases of a Two-Dimensional Bose Gas in an Optical Lattice

K. Jiménez-García,[1,2] R. L. Compton,[1] Y.-J. Lin,[1] W. D. Phillips,[1] J. V. Porto,[1] and I. B. Spielman[1,*]

[1]*Joint Quantum Institute, National Institute of Standards and Technology, and University of Maryland, Gaithersburg, Maryland, 20899, USA*

[2]*Departamento de Física, CINVESTAV-IPN, México D.F., 07360, Mexico*

(Received 7 March 2010; published 9 September 2010)

Ultracold atoms in optical lattices realize simple condensed matter models. We create an ensemble of ≈ 60 harmonically trapped 2D Bose-Hubbard systems from a ^{87}Rb Bose-Einstein condensate in an optical lattice and use a magnetic resonance imaging approach to select a few 2D systems for study, thereby eliminating ensemble averaging. Our identification of the transition from superfluid to Mott insulator, as a function of both atom density and lattice depth, is in excellent agreement with a universal state diagram [M. Rigol *et al.*, Phys. Rev. A **79** 053605 (2009)] suitable for our trapped system. In agreement with theory, our data suggest a failure of the local density approximation in the transition region.

DOI: 10.1103/PhysRevLett.105.110401 PACS numbers: 05.30.Jp, 03.75.Hh, 03.75.Lm

Ultracold atoms in optical lattices constitute a highly controllable system that allows the study of lattice models relevant to condensed matter physics; e.g., the Bose-Hubbard (BH) Hamiltonian [1–4]. By increasing the depth of the lattice potential, one can drive an initially Bose-condensed system through a transition from superfluid (SF) to Mott insulator (MI); experiments have pinpointed the lattice depth for this transition in 2D [5] and 3D [6]. The BH model describes homogeneous systems, but trapped ultracold gases are *globally* inhomogeneous, potentially containing multiple, spatially separated phases. For sufficiently large systems this inhomogeneity can be understood using the local density approximation (LDA), where each region of the system is treated as being *locally* homogeneous. Rigol *et al.* [7] introduced a "universal state diagram" for harmonically trapped systems describing the configuration of spatially separated SF and MI phases, coexisting under harmonic confinement. We present measurements on 2D trapped systems and identify the transition from SF to MI as a function of lattice depth and atom number; the resulting experimental state diagram, Fig. 1, is in good agreement with the quantum Monte Carlo (QMC) predictions going beyond LDA, [7].

The BH Hamiltonian models bosons in a lattice potential, here realized with ultracold ^{87}Rb atoms in an optical lattice. The BH model includes only pairwise on-site interactions (interaction energy U) and nearest-neighbor tunneling (tunneling matrix element t). At zero temperature this model predicts a SF phase and MI phases with integer occupation $n = 1, 2, 3\ldots$ per lattice site, in terms of the ratio U/t and the chemical potential μ. The interaction strength is described by U/t while the density is largely controlled by μ/t. For weak interactions (small U/t) the system is SF, while for U/t larger than a critical value $(U/t)_c$ the system can enter a MI phase. For $U/t \gg (U/t)_c$, the phases alternate between SF and MI, increasing in density as μ increases [8].

The homogeneous BH model is not applicable to current experiments on ultracold atoms, owing to their harmonic trapping potential. The BH Hamiltonian for a lattice with period d superimposed on a symmetric harmonic trap is [1]

$$H = -t\sum_{\langle i,j\rangle} \hat{b}_i^\dagger \hat{b}_j + \frac{U}{2}\sum_i \hat{n}_i(\hat{n}_i - 1) + \sum_i (\epsilon i^2 - \mu)\hat{n}_i,$$

where $\hat{b}_i^\dagger$ is the creation operator of a boson at site i and $\langle i, j\rangle$ constrains the sum to nearest-neighbor tunneling. The

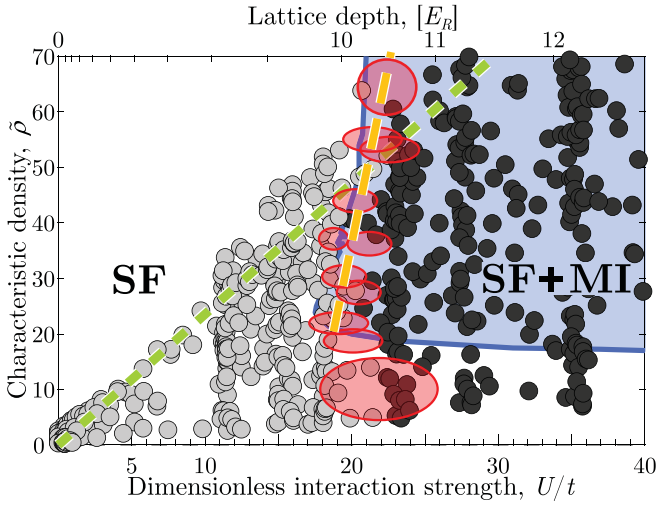

FIG. 1 (color). State diagram for a harmonically trapped 2D Bose gas. The blue line shows the QMC predicted [7] first appearance of MI. The transition was measured at various N_{2D} from $f(U/t)$ data (e.g., of Fig. 4, whose data were taken along the green dashed path). The ovals denote the measured transition boundary; their sizes represent the uncertainties in $\tilde{\rho}$ and $(U/t)_c$. The small circles indicate individual measurements and are shaded according to the side of the transition on which they are. The yellow dashed line is a fit to the measured boundary for $\tilde{\rho} > 20$; this nonvertical [$\theta_{\text{exp}} = 85.5(27)°$ from horizontal], suggests a breakdown of the LDA.

parameter $\epsilon = m\omega^2 d^2/2$ describes the harmonic potential (m is the atomic mass and $\omega = 2\pi\nu$ is the trap frequency).

In the LDA, $\mu - \epsilon i^2 = \mu_i$ is assumed to be constant over an extended region, producing a local chemical potential μ_i; the system's properties are then computed with the homogeneous BH Hamiltonian. The LDA explains the evolution of a SF system into a nested collection of alternating SF and MI shells as U/t increases [9], observed using a magnetic resonance imaging (MRI) approach on a 3D system [10], by measuring collisional shifts [11], and more recently by direct imaging on a single 2D system [12].

The inhomogeneity from the trap leads, for sufficiently large ϵ, to a breakdown of the LDA: the trap potential can increase the critical value $(U/t)_c$, where MI first appears [7]. Using a site-decoupled mean field theory (MFT) calculation for our trapped system [13], we found that a proximity-like effect [14] stabilizes the SF in regions where the LDA-MFT predicts MI.

For a $T = 0$ 2D trapped system, the three parameters U/t, ϵ, and atom number N_{2D}, fully specify the quantum state of the system, even with coexisting regions of SF and MI. Somewhat surprisingly, only two independent variables are sufficient [7], U/t and a characteristic density $\tilde{\rho} = N_{2D}\epsilon/t$. By monitoring the dependence of condensate fraction f on $\tilde{\rho}$ and U/t [5], we measure the state diagram for 2D systems in an optical lattice (Fig. 1).

We partition a 3D Bose-Einstein condensate (BEC) into ≈ 60 nearly independent 2D systems using a 1D optical lattice along $\hat{z}$ (Fig. 2). Additional optical lattices along $\hat{x}$ and $\hat{y}$ produce a BH Hamiltonian for each 2D system. At higher temperatures than those discussed here, the first appearance of $n = 1$ MI domains was reported in Ref. [5]. That ensemble measurement could not distinguish between 2D systems with different $\tilde{\rho}$. To overcome the ensemble averaging, we developed a MRI approach to slice out a small subset of nearly identical 2D systems and measure their momentum distribution. We also use matter-wave focusing [15] to more accurately identify the condensate.

We prepare a 2×10^5 atom ^{87}Rb BEC [16] with no discernible thermal component, in the $|F = 1, m_F = 1\rangle$ state in a harmonic trap with measured trap frequencies $\{\nu_x, \nu_y, \nu_z\} = \{23.2(5), 27.4(3), 42.8(9)\}$ Hz [17]. The BEC is confined 620 μm above the zero of a quadrupole magnetic field at the intersection of a pair of 1064 nm laser beams, propagating along $\hat{x}$ and $\hat{y}$, with waists ($1/e^2$ radii) of ≈ 55 μm. At the center of the BEC the magnetic field is $B_0 = 193$ μT, with Zeeman shift $g\mu_B B_0/h = 1.35$ MHz. The magnetic potential, nearly linear along $\hat{z}$ with a gradient of 2.180(4) kHz/μm, cancels gravity and adds a harmonic antitrapping potential in the $\hat{x} - \hat{y}$ plane for our $m_F = 1$ atoms.

We load the BEC into a 3D optical lattice at the intersection of three pairs of linearly polarized nearly counter propagating laser beams from a $\lambda = 810$ nm Ti:sapphire laser [18]. These beams form independent 1D optical lattices along $\hat{x}$, $\hat{y}$ and $\hat{z}$. The $\hat{z}$ lattice, set to a final depth of 24 E_R, partitions the 3D BEC into 2D systems; the depth of the $\hat{x} - \hat{y}$ lattice ranges from 0 to 20 E_R and determines the parameter U/t. Together all confining potentials determine ϵ. The recoil energy is $E_R = \hbar^2 k_R^2/2m = h \times 3.4$ kHz, where $k_R = 2\pi/\lambda$. The lattices are turned on from zero intensity in 100 ms with a half-Gaussian intensity ramp (rms width of 37 ms). This time scale was chosen to be adiabatic with respect to interactions and all relevant single particle energy scales [5,19]. We measure lattice depth to within $\approx 2\%$ by pulsing on each lattice separately for 4 to 6 μs and observing the resulting atom diffraction [5,20].

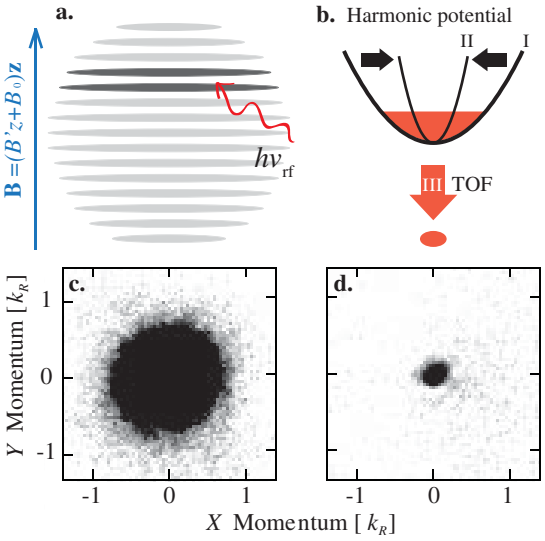

FIG. 2 (color). (a) Our 3D BEC is divided into 2D systems by an optical lattice in the presence of a linear magnetic field gradient, both aligned along the $\hat{z}$ direction. We use a MRI technique to selectively address a small subset of 2D systems. (b) Matter-wave focusing is used to better resolve the SF phase of the 2D Bose gas; shown is a schematic of the focusing of a single 2D system after free evolution during TOF. (c)–(d) We compare the measured atom distribution (approximating the momentum distribution) of the ensemble of ≈ 60 2D systems without focusing (c) with that of the addressed 2D systems in the $m_F = 0$ sublevel with focusing (d), both with an $\hat{x} - \hat{y}$ lattice at $9.5E_R$.

We implemented a MRI approach to address a small number of adjacent, nearly identical, 2D systems [Fig. 2(a)]. A rf magnetic field B_{rf} transfers atoms from $m_F = 1$ to $m_F = 0$ and -1. We choose B_{rf} to maximize the transfer into $m_F = 0$ using a 400 μs Blackman pulse (perfect transfer to $m_F = 0$ is impossible for our 3 level system). The 2 kHz rms spectral width of this pulse, combined with the magnetic field gradient gives a 0.9 μm rms spatial resolution (≈ 2 sites).

Following the rf pulse, the lattices are ramped off with exponentially decreasing ramps (400 μs time constant)—nearly adiabatic with respect to single particle energy scales in the optical lattice—approximately mapping the occupied crystal momentum states to free momentum

states [21,22]. We concurrently remove the optical dipole trap in <1 μs and the atoms then expand for a 18.1 ms time of flight (TOF). During part of TOF, a magnetic field gradient separates the three m_F components. We then detect the final spatial distribution of all three components using resonant absorption imaging, which gives the distribution of each spin component separately. The $m_F = 0$ distribution directly measures the momentum composition of the nearly identical 2D systems selected by the rf pulse, virtually eliminating the inhomogeneous averaging that is present in the $m_F = 1$ distribution [see Fig. 2(c)]. The fact that $m_F = 0$ atoms are insensitive to gradients in magnetic fields ensures no distortions to the momentum distribution due to field gradients.

Absorption images after TOF can differ from the *in situ* momentum distributions for two primary reasons: (i) interactions during TOF and (ii) finite TOF, here 18.1 ms. We mitigate each of these effects: (i) The already weak interactions during TOF for the small number of atoms transferred into $m_F = 0$ are further reduced by the rapid expansion along $\hat{z}$ after release from the tightly confining vertical lattice; (ii) we used a matter-wave focusing technique: a temporal atom lens that images the *in situ* momentum distribution at a finite TOF [15]. To focus the atoms we increase the harmonic trapping frequency by a factor of about 3, by linearly ramping the intensity of our 1064 nm dipole trap in 200 μs, and then holding for 400 μs (during the rf pulse) just before TOF.

After TOF, our 3D BEC has a 57 μm Thomas-Fermi (T-F) radius. When partitioned into an ensemble of 2D systems the TOF radius decreases to 47 μm [Fig. 2(c)]. For the extracted 2D systems that radius is 20 μm. Figure 2(d) illustrates the final reduction to 11 μm with focusing.

We carefully the calibrated atom number by measuring the *in situ* 1D density profile $n(z)$, of our 3D BEC using the MRI technique [Fig. 3(a)]. The T-F radius $R_z = 8.2(2)$ μm gives atom number $N_{\text{T-F}} = 1.8(4) \times 10^5$; direct integration of $n(z)$ gives $N_{\text{int}} = 1.89(5) \times 10^5$; measurement of absorption by all atoms after TOF gives $N_{\text{abs}} = 1.90(5) \times 10^5$. These measurements are consistent with a combination of shot-to-shot number fluctuations and number measurement uncertainty of $\sim$3%. We confirm this by loading the BEC into the 1D optical lattice along $\hat{z}$, and again measuring $n(z)$. The density profile expands along $\hat{z}$ [Fig. 3(b), circles] but the integrated atom number $N_{\text{int}} = 1.84(5) \times 10^5$ remains constant. Figure 3(b) also shows the measured temperature T in a 1D optical lattice as a function of z (squares). $T = 15(3)$ nK is nearly uniform over all significantly occupied lattice sites, indicating that the 2D systems taken together are effectively in thermal equilibrium.

We set U/t by tuning the $\hat{x} - \hat{y}$ lattice depth, and $\tilde{\rho}$ by rf-selecting 2D systems with the desired atom number from among the $\approx$60 available systems. As a result, each measured momentum distribution corresponds to a single point on the $U/t - \tilde{\rho}$ plane; we use f to distinguish between the SF and MI phases.

We define f as the fraction of atoms in the sharp, focused feature in the momentum distribution. We fit the broad background, present due to thermal effects and quantum depletion, including atoms in the MI phase, to the thermal distribution of noninteracting classical particles in a 2D sinusoidal band; in the shallow lattice limit the width of this distribution is interpreted as temperature: $T = 0.9(2)t/k_B$ [5]. We smoothed the fit function in a region

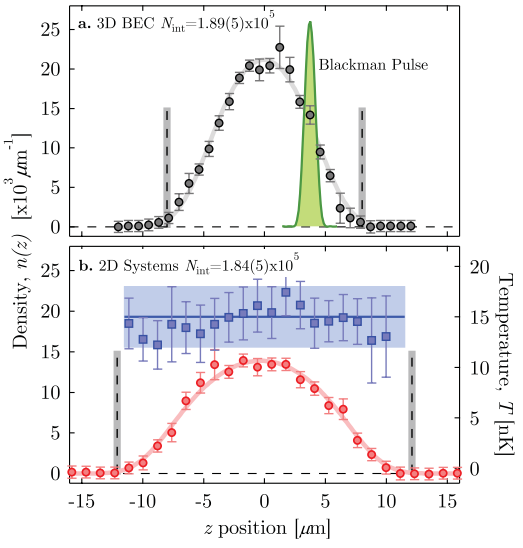

FIG. 3 (color). Density profile $n(z)$ for: (a) a 3D BEC and (b) an ensemble of 2D systems. The atom number calculated from the *in situ* T-F radius $R_z = 8.2(2)$ μm is $N_{\text{T-F}} = 1.8(4) \times 10^5$. The vertical dashed lines indicate the T-F radius from our fit. Continuous lines show a fit to the *in situ* 1D density profile $n(z)$. The temperature of the selected 2D systems [squares in (b)] is displayed on the right axis, as a function of position along $\hat{z}$. On average $T = 15(3)$ nK.

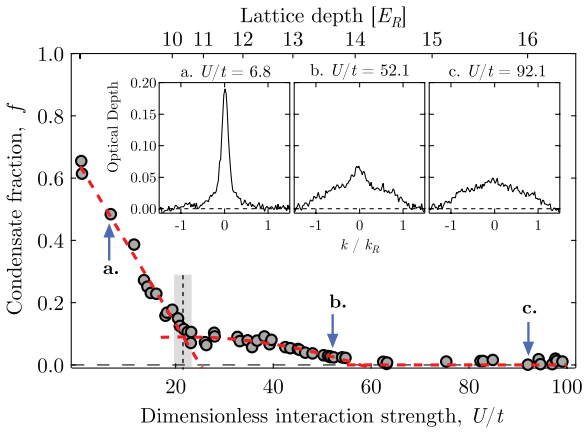

FIG. 4 (color). 2D condensate fraction for $N_{\text{2D}} \approx 3500$ measured through the SF to MI transition. The red dashed curves are described in the text. The insets (a)–(c) display the average momentum distribution $n(k) = [n_x(k) + n_y(k)]/2$ at different U/t, where $n_x(k)$ is the momentum distribution integrated over y and likewise for $n_y(k)$. We identify the formation of the first MI region at $U/t = 21(2)$. $f \approx 0$.

within $0.1k_R$ of the edge of the Brillouin zone to account for nonadiabaticities in the lattice turn off near the band edge [21]. We exclude a disk with $0.16k_R$ radius around the condensate feature from the fit and identify the condensate as the atoms that remain within the disk after subtracting the background fit. (We associate $f > 0$ with existence of SF regions as is conventional.)

Figure 4 shows f versus U/t for 2D systems with $N_{2D} \approx 3500$ and an initial temperature $T = 0.9(2)t/k_B$ (as interactions become increasingly important, this temperature increases in units of t), a factor of 2 lower than that in Ref. [5] where $f \lesssim 0.4$ and $T \approx 2t$. We identify three distinct regions. For small U/t, f rapidly decreases (Fig. 4, fit to a line) until $f \approx 0.12$ and $(U/t)_c = 21(2)$ where the slope changes markedly. We associate this feature with the first appearance of a MI and the subsequent decay (Fig. 4, fit to a parabola) with the spatial growth of the MI regions. This association is supported by our MFT calculation. For $U/t > 60$, f is indistinguishable from zero. The critical point for appearance of MI $(U/t)_c = 21(2)$ is consistent with trapped system QMC calculations ($(U/t)_c = 20.5$ at $\tilde{\rho} = 53$) [7]. A similar analysis at $\tilde{\rho} \approx 20$ gives $(U/t)_c = 19(2)$, consistent with the past measurement ($(U/t)_c = 15.8(20)$) [5] and trapped system QMC ($(U/t)_c = 20$ at $\tilde{\rho} = 20$) [7,23], whereas homogeneous system QMC calculations [24–26] gives $(U/t)_c = 16.5$.

Our measurements are summarized in Fig. 1. We extracted f from about 1300 images with $\tilde{\rho}$ and U/t each up to 100 [27]. The green dashed line corresponds to a constant atom number ($N_{2D} \approx 3500$) path in the $U/t - \tilde{\rho}$ plane. Each red oval marks the measured value of $(U/t)_c$ when MI first appears for a different N_{2D}, its width and height represent the uncertainty in the measurement [28]. All data points are shaded according to the side of the transition on which they are: SF in light grey and the presence of MI in dark grey.

Figure 1 also displays the QMC state diagram [7]. The continuous curve shows the expected first appearance of a MI; the agreement with this result is obtained with no adjustable parameters. The deviation from vertical of the upper portion of this curve, reproduced by the data, differs from the LDA prediction. Linear fits for the measured (yellow dashed line in Fig. 1) and predicted transition boundaries, for $\tilde{\rho} > 20$, intersect the horizontal axis at angles $\theta_{exp} = 85.5(27)°$ and $\theta_{QMC} = 83.7(3)°$ respectively, suggesting the breakdown of LDA near the transition. The universal character of the state diagram is revealed in the $U/t - \tilde{\rho}$ plane: it is independent of N_{2D} or ϵ and of the validity of the LDA [7]. The discrepancy for $\tilde{\rho} < 15$ is expected due to increased sensitivity to thermal effects at low density where the SF transition temperature is extremely low.

During the preparation of this Letter we learned of a similar experimental technique applied to a 2D Bose system in the higher temperature BKT regime [29].

We appreciate enlightening conversations with C. Chin and J. K. Freericks; and we thank K. Mahmud and R. T. Scalettar for discussions and for sharing their QMC data (reproduced in Fig. 1). This work was partially supported by grants from the ONR, the ARO with funding from the DARPA OLE program, and the NSF through the JQI Physics Frontier Center; K. J. G. thanks CONACYT and R. L. C. thanks the NIST/NRC program.

*ian.spielman@nist.gov

[1] D. Jaksch *et al.*, Phys. Rev. Lett. **81**, 3108 (1998).
[2] M. Greiner *et al.*, Nature (London) **415**, 39 (2002).
[3] M. Köhl *et al.*, J. Low Temp. Phys. **138**, 635 (2005).
[4] I. B. Spielman, W. D. Phillips, and J. V. Porto, Phys. Rev. Lett. **98**, 080404 (2007).
[5] I. B. Spielman, W. D. Phillips, and J. V. Porto, Phys. Rev. Lett. **100**, 120402 (2008).
[6] J. Mun *et al.*, Phys. Rev. Lett. **99**, 150604 (2007).
[7] M. Rigol, G. G. Batrouni, V. G. Rousseau, and R. T. Scalettar, Phys. Rev. A **79**, 053605 (2009).
[8] M. P. A. Fisher, P. B. Weichman, G. Grinstein, and D. S. Fisher, Phys. Rev. B **40**, 546 (1989).
[9] In the LDA, the critical value $(U/t)_c$ at which MI first appears, becomes independent of system size for sufficiently large values of μ/t.
[10] S. Fölling *et al.*, Phys. Rev. Lett. **97**, 060403 (2006).
[11] G. K. Campbell *et al.*, Science **313**, 649 (2006).
[12] N. Gemelke, X. Zhang, C.-L. Hung, and C. Chin, Nature (London) **460**, 995 (2009).
[13] K. Sheshadri, H. R. Krishnamurthy, R. Pandit, and T. V. Ramakrishnan, Europhys. Lett. **22**, 257 (1993).
[14] M. Tinkham, *Introduction to Superconductivity* (McGraw-Hill, New York, 1996), 2nd ed.
[15] A. H. van Amerongen *et al.*, Phys. Rev. Lett. **100**, 090402 (2008).
[16] Y.-J. Lin *et al.*, Phys. Rev. A **79**, 063631 (2009).
[17] Uncertainties reflect the uncorrelated combination of one-standard deviation statistical and systematic uncertainties.
[18] The vertical lattice beams intersect at 164(1)°, giving a ≈420 nm lattice. They differ in frequency from the $\hat{x} - \hat{y}$ lattice beams by ≈160 MHz, while the cross polarized $\hat{x} - \hat{y}$ beams differ from each other by ≈3 MHz.
[19] T. Gericke *et al.*, J. Mod. Opt. **54**, 735 (2007).
[20] We calculate lattice depth from the pulse duration required for the 0th and 1st orders to be equally populated.
[21] D. McKay, M. White, and B. DeMarco, Phys. Rev. A **79**, 063605 (2009).
[22] This introduces essentially no additional errors in f.
[23] S. Wessel, F. Alet, M. Troyer, and G. G. Batrouni, Phys. Rev. A **70**, 053615 (2004).
[24] W. Krauth and N. Trivedi, Europhys. Lett. **14**, 627 (1991).
[25] N. Elstner and H. Monien, arXiv:cond-mat/9905367.
[26] Y. Kato, N. Kawashima, and N. Trivedi (private communication).
[27] Our adiabaticity criterion for loading may break down when we enter into the regime of high U/t.
[28] The uncertainty in $\tilde{\rho}$ takes into account the width of the rf selection pulse [Fig. 3(a)].
[29] E. A. Cornell (private communication).